# Innovative Narwhal MPPT with Feed forward Decoupling for Enhanced Solar Grid Integration

**Ravi Shankar Pranavasundaram[1,*], Gokul Chandrasekaran[2]**
*[1]Department of Mechatronics Engineering, Nehru Institute of Engineering and Technology, Coimbatore 641105, Tamil Nadu, India*
*[2]Department of Electronics and Communication Engineering, Karpagam Institute of Technology, Coimbatore 641105, Tamil Nadu, India*
*[*]rraviik7@gmail.com; gokulvlsi@gmail.com*

***Abstract*—This paper presents a novel hybrid maximum power point tracking (MPPT) strategy that integrates the Narwhal optimisation algorithm (NWO) with a feed forward decoupling control (FFDC) scheme for a grid-connected single-ended primary-inductor converter (SEPIC) inverter-based photovoltaic (PV) system. Conventional and metaheuristic MPPT methods often exhibit a trade-off between convergence speed, tracking accuracy, and robustness under partial shading and dynamic irradiance. The proposed NWO-FFDC approach addresses these limitations by leveraging the efficient global search capabilities for rapid MPP localisation and the precise control of the FFDC for stable grid integration. Simulation results demonstrate that the NWO-FFDC achieves a tracking efficiency of 99.2 %, reduces steady-state oscillations to 0.5 W, and achieves convergence within 42 ms. Furthermore, inverter performance analysis confirms that the proposed controller maintains DC link voltage stability at 700 V with minimal droop and delivers AC power to the grid with a total harmonic distortion (THD) of only 2 % under all conditions, ensuring full compliance with IEEE 1547 standards. These results establish NWO-FFDC as a superior solution, offering improved tracking precision, faster dynamic response, and improved grid compatibility for next-generation PV systems.**

***Index Terms*—PV integrated grid; Narwhal MPPT; Feed forward decoupling; SEPIC converter; Voltage source inverter.**

## I. INTRODUCTION

The global energy landscape is undergoing a profound transformation, driven by the urgent need for sustainable and clean power sources. Among renewable technologies, photovoltaic (PV) systems have emerged as a cornerstone, experiencing unprecedented annual growth of 30 % to 40 % over the past decade [1]–[4]. This surge is largely fuelled by grid-integrated solar installations, which have simultaneously driven technological advancements and substantial cost reductions in PV modules and power electronic interfaces.

A critical determinant of the economic viability of a grid-connected PV plant is the efficiency and reliability of its power conversion chain. While the specifications of PV modules are fundamental, the performance of the converters and inverters that interface with the distribution network is paramount. Key factors such as rated power, DC link voltage stability, and sophisticated inverter control strategies directly influence the energy yield and operational lifespan of the installation [5]–[9]. Furthermore, stringent compliance with international grid codes (e.g., IEEE 1547), which mandate power quality, harmonic distortion limits, and anti-islanding protection, is a nonnegotiable requirement for seamless grid integration.

The inherent nonlinear characteristics of PV arrays, coupled with their susceptibility to external atmospheric conditions, such as partial shading and rapidly changing irradiance, pose a significant challenge. These conditions create complex, multimodal power-voltage (P-V) curves with multiple local maxima, severely hindering the ability to harvest maximum available power. Therefore, the maximum power point tracking (MPTT) controller is the most critical intelligence unit in any PV system, tasked with continuously and accurately locating the global maximum power point (GMPP) in real time [10], [11].

Conventional MPPT techniques, such as perturb and observe (P&O) and incremental conductance (INC), are widely adopted due to their simplicity. However, they exhibit inherent limitations, including oscillatory behaviour around the MPP under steady-state conditions, poor dynamic response during rapid environmental changes, and a fundamental inability to distinguish the global peak from local peaks under partial shading. To address these drawbacks, several metaheuristic algorithms have been explored for their superior global search capabilities. Although these approaches improve global peak detection, they introduce new trade-offs, including slower convergence speeds, residual steady-state oscillations, and higher computational overhead, which restrict their effectiveness in real-time, grid-tied PV applications.

To overcome these challenges, this paper introduces a novel hybrid MPPT strategy that integrates the Narwhal optimisation algorithm (NWO) with a feedforward decoupling control (FFDC) scheme. NWO is particularly suited for the complex, multimodal P-V characteristics of PV systems due to its dynamic balance factor and unique whale-fall mechanism, which significantly enhance its ability to escape local maxima and achieve rapid convergence to the GMPP under partial shading scenarios.

Manuscript received 25 May, 2025; accepted 2 August, 2025.

Complementing this, the FFDC framework ensures precise decoupled control of active and reactive power injected into the grid, thereby minimising total harmonic distortion (THD) and maintaining stable DC link voltage. Implemented on a single-ended primary-inductor converter (SEPIC) for its versatile voltage conversion capability, the proposed NWO-FFDC approach is validated through extensive simulations under static, dynamic, and partial shading conditions. The results demonstrate best-in-class performance in terms of tracking efficiency, convergence speed, steady-state stability, and power quality, thus establishing the NWO-FFDC as a new benchmark for next-generation grid-connected PV systems.

## II. Related Works

Particle swarm optimisation (PSO) and hybrid PSO with conventional MPPT [12], [13] offer rapid convergence and reduced oscillations compared to P&O.

Optimising MPPT approaches using fuzzy logic combined with metaheuristic methods has demonstrated superior performance in standalone PV systems under low and high irradiation conditions, as well as during transient states[14]. Adaptive neuro-fuzzy inference systems (ANFIS) for MPPT control along with two-axis sun tracking has been developed for the grid integrated PV system. This integration ensures effective tracking of the MPP while improving adaptability, response speed, and output precision [15].

Enhancing the conventional hybrid metaheuristic algorithm along with solar axis tracking for grid-integrated PV systems has shown promising results. Simulations indicate that this approach significantly increases energy harvesting and overall efficiency compared to traditional methods [16].

Researchers have shown that fuzzy MPPT algorithms, optimised with genetic algorithm (GA) [17], indicate superior performance compared to P&O - proportional-integral (PI) controllers. Specifically, the fuzzy PI-based MPPT algorithm outperforms the P&O - PI controller. For real-time evaluations, a boost converter with hybrid neural network PSO-radial basis function (RBF) approaches has been formulated. In this, PSO was used to minimise root mean square error (RMSE) error. The proposed system achieved quick convergence and high efficiency performance, even under partial shading conditions (PSC) [18].

Additionally, a combined approach of an artificial bee colony (ABC) and ANFIS-based MPPT was introduced. This approach ensures anti-islanding network security [19].

A synergistic approach of blending an optimised P&O algorithm with ABC has been devised for solar plants that function in PSC. In this method, the ABC identifies the global MPP (GMPP), with subsequent fine-tuning by the P&O algorithm. The outcomes demonstrate significant reduction in fluctuations during steady-state operation, making it particularly suitable for partial shade conditions (PSC). Moreover, this approach showcases a rapid payback period and delivers remarkable efficiency.

In a groundbreaking fusion of a BAT fuzzy controller for grid-tied PV installations, it has been proposed. In this, BAT autonomously uncovers the optimal controller value, fine-tuned further by the fuzzy logic (FL) system. The outcomes reveal swift convergence, enhanced efficiency, and reliable performance, even under challenging conditions such as PSC [20].

An innovative MPPT strategy based on harmony search algorithm (HGO) optimisation was proposed. Comparisons between various existing algorithms HGO reveal high efficacy with minimum tracking time [21]. A novel Harris hawk optimisation (HHO) MPPT approach proved to be effective in monitoring global MPPT under all conditions, exhibiting superior performance in achieving MPP and rapid convergence [22]. Similarly, salp swarm optimisation (SSO) depicts improved tracking and higher stability compared to traditional approaches such as PSO, etc. Analytical investigation further confirms the robustness and sensitivity of SSO. The proposed manta ray foraging optimisation (MRFO) algorithm demonstrated robust global MPP tracking under PSC and exhibits superior performance [23].

Despite notable progress in MPPT strategies [24], most existing methods still exhibit limited adaptability under PSC. Such constraints often lead to tracking inefficiency, slower convergence, and premature settling at local maxima. Therefore, an approach that simultaneously improves energy harvesting efficiency and grid compliance would represent a significant step forward in the practical deployment of high performance PV systems.

In response to this research gap, the present work introduces a pioneering MPPT strategy that integrates the Narwhal optimisation algorithm (NWO) with feed forward decoupling control (FFDC). The NWO, with its dynamic balance factor and whale-fall mechanism, provides superior global search capability, enabling rapid and reliable convergence to the GMPP in complex environmental scenarios. On the grid side, the FFDC framework ensures robust decoupled control of active and reactive power, thereby minimising THD and maintaining stable DC link voltage. This synergistic combination not only enhances the efficiency of energy extraction from PV arrays, but also guarantees stable grid integration. Extensive simulation studies validate the proposed NWO-FFDC technique, confirming its ability to maximise energy output, improve dynamic response, and maintain stability under diverse operating conditions. Comparative analysis with existing MPPT algorithms further highlights its superior tracking precision and robustness, establishing it as a significant advancement in the development of grid-connected PV systems.

## III. Methodology

This section presents the modelling and control framework adopted for the proposed system. First, the PV array and SEPIC converter are modelled to define the power conversion stage. Next, the Narwhal optimisation algorithm (NWO) is integrated with feed forward decoupling control (FFDC) to achieve accurate MPPT and stable grid synchronisation.

### *A. Solar Panel*

Solar cells, also known as photovoltaic (PV) cells, serve as the foundational components of solar panels. The internal mechanism of a PV cell is illustrated in the equivalent

circuit shown in Fig. 1.

Figure 1 illustrates a simplified depiction of a photovoltaic (PV) cell, consisting of a diode connected in parallel with an ideal current source. The current source produces a current that corresponds to the intensity of solar radiation falling on the cell.

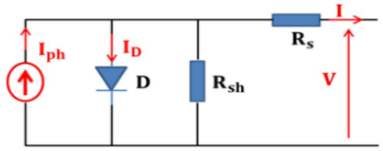


Fig. 1. PV Cell - Equivalent circuit [20].

Thus, the current/voltage of a PV cell is depicted in (1) and (2):

$$I = Isc - Io\left(\exp\left(\frac{q\left(V+IR_s\right)}{nkT}\right)-1\right)-\left(\frac{V+IR_s}{R_p}\right), \quad (1)$$

$$Voc = \frac{kT}{q}ln\left(\frac{Isc}{Io}+1\right). \quad (2)$$

### B. Converter Design

The SEPIC converter stands out as a highly adaptable and efficient DC converter that delivers stable and regulated voltage across a diverse array of applications [25]. Its design facilitates the maintenance of continuous input and output currents, effectively minimising output voltage ripple, making it particularly suitable for powering sensitive electronic devices.

At its core, converter comprises an inductor, a capacitor, and a switch. Notably, it incorporates two distinct capacitors - one positioned on the input side and another on the output side - endowing it with the distinctive capability to handle both step-up and down- voltage conversion tasks. The circuit diagram that illustrates the configuration of the SEPIC converter is depicted in Fig. 2.

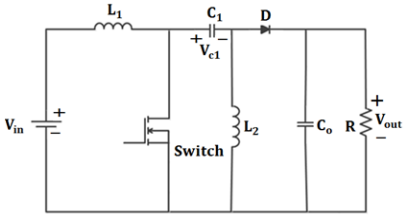


Fig. 2. Circuit diagram of the SEPIC converter.

The operation of the proposed converter can be summarised as follows.

In the initial stage, as the switches are shut, the inductor accumulates energy from the input voltage ($V_{in}$) within its magnetic field.

During the second phase, when the switches are open, the energy stored in the inductor flows into the output capacitor ($C_o$) and the load. Consequently, the output voltage ($V_{out}$) will either rise or fall relative to the input voltage, depending on the duty cycle of the switches.

The standout characteristic of the SEPIC converter lies in its ability to transfer energy to both the output capacitor and the input capacitor ($C_{in}$) during its operational cycle. This distinctive feature enables it to perform voltage conversion, facilitating both step-up and step-down functions, all without the necessity of a transformer.

Thus, the voltage gain ($V_G$) of the converter can be

$$V_0 = \frac{D}{1-D}V_{in}, \quad (3)$$

where D is the duty cycle.

This flexibility makes SEPIC highly suitable for PV applications with variable irradiance and temperature.

### C. Narwhal Optimisation (NWO)

NWO is selected for this application because of its demonstrated superiority in solving complex optimisation problems with multimodal characteristics, such as those presented by P-V curves under partial shading. Compared to other metaheuristics, such as PSO and whale optimisation algorithm (WOA,) NWO features a more dynamic balance factor. The NWO is chosen for MPPT due to its superior ability to escape local maxima and rapidly converge to the global maximum power point (GMPP). Its two distinctive features are the following:

1. Dynamic balance factor - enabling adaptive switching between exploration and exploitation;
2. Whale-fall mechanism - ensuring population diversity and preventing premature convergence.

Compared to PSO and WOA, NWO requires fewer parameters, offers faster convergence, and minimises oscillations, making it more practical for real-time grid-connected PV systems. Thus, the formulation of NWO is explained in the following.

*– Initialisation*

In the NWO topology, the whale is modelled as a search agent. The search process is driven by updating its position within the search space, which is represented by a position vector. The matrix representing the location of the search agents is

$$Y = \begin{matrix} y_{1,1} & y_{1,2} & y_{1,dim} \\ y_{2,1} & y_{2,2} & y_{2,dim} \\ \vdots & \vdots & \vdots \\ y_{n,1} & y_{n,2} & y_{n,dim} \end{matrix}. \quad (4)$$

The fitness value can be expressed as in (5)

$$F_x = \begin{bmatrix} f\left(y_{1,1}, y_{1,2}, ..., y_{1,dim}\right) \\ f\left(y_{2,1}, y_{2,2}, ..., y_{2,dim}\right) \\ \vdots \\ f\left(xy_{n,1}, y_{n,2}, ..., xy_{n,dim}\right) \end{bmatrix}. \quad (5)$$

This algorithm involves transitioning between exploration and exploitation stages to effectively reach a mutually beneficial agreement. In the exploration stage, the balance factor (BF) could start with a relatively high value. In the exploitation stage, with a lower value of *Bf*, the algorithm would tend to the optimal solution based on the exploration results. Thus, the balance factor plays a significant role in determining the overall performance and behaviour of the algorithm during negotiations

$$Bf = Bo \times \left(1 - \frac{t}{2T}\right), \tag{6}$$

where $t$ is the iteration (current), $T$ is the iteration (maximum), and $Bo$ is the random number (0, 1).

If $Bf > 0.5$, then it is in the exploitation stage, otherwise it executes the exploitation stage.

*– Exploration phase*

Narwhal's position update is as follows:

$$\begin{cases} X_{i,j}^{t+1} = X_{i,Pj}^{t} + \left(X_{r,Pr}^{t} - X_{i,Pj}^{t}\right) \times (1 + r_2) \times sin(2\pi r_2), j = even, \\ X_{i,j}^{t+1} = X_{i,Pj}^{t} + \left(X_{r,Pr}^{t} - X_{i,Pj}^{t}\right) \times (1 + r_2) \times cos(2\pi r_2), j = odd, \end{cases} \tag{7}$$

where $X^{t+1}{}_{i,j}$ is the position of the $i^{\text{th}}$ Narwhal on $j^{\text{th}}$ dimension, $P_j$ and $P_r$ are integers within [1, dim], $X^{t}{}_{i,Pj}$ and $X^{t}{}_{r,Pr}$ is the present position of the $i^{\text{th}}$ and $r^{\text{th}}$ Narwhal, and $r$ and $r_2$ are random numbers (0, 1).

Based on the chosen dimension, the updated position mirrors the behaviours of a Narwhal whale while swimming or diving.

*– Exploitation phase*

The exploitation phase is crucial to refine the solutions found during the exploration phase. This phase involves local search strategies where Narwhal converges on the best solutions identified so far:

$$X_i^{t+1} = r_3 X_{best}^{t} - r_4 X_i^{t} + C_1 \times L \times \left(X_r^{t} - X_i^{t}\right), \tag{8}$$

$$C_1 = 2r_4 \times \left(1 - \frac{t}{T}\right). \tag{9}$$

$L$ is the random number consistent and can be calculated as follows:

$$L = 0.05 \times \frac{u \times \sigma}{|v|^{1/\beta}}, \tag{10}$$

$$\sigma = \left( \frac{r(1+\beta) \times sin(\pi\beta/2)}{r\left((1+\beta)/2\right) \times \beta \times 2^{(\beta-1)/2}} \right), \tag{11}$$

where $u$ and $v$ are random numbers and $\beta$ - 1.5.

*– Whale fall*

To ensure a constant population size, the positions of the Narwhals and the step sizes of their movements are used to determine their updated positions. The corresponding formula is given as

$$X_i^{t+1} = r_5 X_i^{t} - r_6 X_r^{t} + r_7 X_{step}, \tag{12}$$

where $r_5$, $r_6$ and $r_7$ are random numbers.

$X_{step}$ is the step size and can be depicted as

$$X_{step} = (ub - lb) \exp\left(-C_2 \frac{t}{T}\right), \tag{13}$$

where $C_2$ is the step size factor

$$C_2 = 2Wf \times n \tag{14}$$

and $ub$ and $lb$ are the upper and lower bounds of the variables.

The probability of a Narwhal whale falling is as follows:

$$W_f = 0.1 - 0.05 \frac{t}{T}. \tag{15}$$

The likelihood of a Narwhal encountering danger diminishes as it progresses from the initial stage to the final stage of optimisation. This suggests that as the Narwhal approaches its food source, the probability of survival increases. The pseudocode of the proposed topology is depicted below (Algorithm 1).

Algorithm 1. Pseudocode of the NWO algorithm.

1.Initialise the population of Narwhals with random duty cycles.
2. Evaluate fitness (PV power) for each candidate.
3. Select the best candidate as the best global one.
4. For each iteration:
  a. Update the balance factor.
  b. If exploration phase → update positions randomly.
  c. If exploitation phase → refine search near best solution.
  d. Apply the whale-fall mechanism with certain probability.
  e. Evaluate new fitness values.
  f. Update global best if improved.
5. Repeat until convergence or maximum iterations.
6. Output optimal duty cycle corresponding to GMPP.

Figure 3 depicts the flowchart of the proposed NWO algorithm.

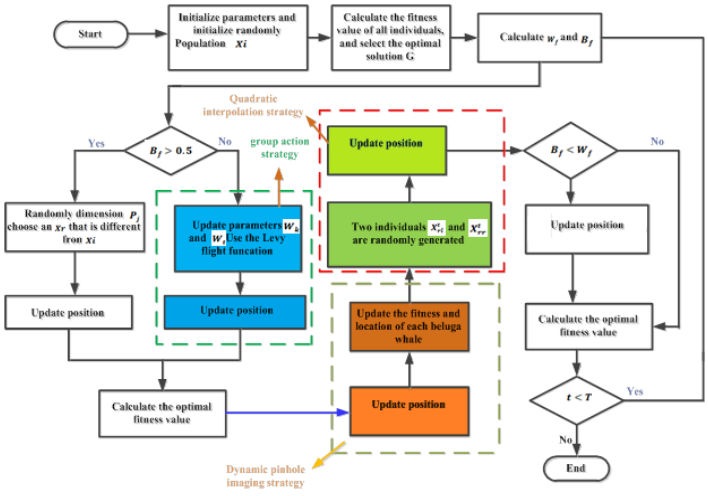


Fig. 3. Narwhal optimisation flowchart.

*D. Inverter Design*

The primary objective of an inverter in a grid-connected setup is to deliver power with high efficiency, minimal distortion, and precise synchronisation with the voltage and frequency of the grid. The mathematical expressions for the AC output voltages in a 3Φ inverter are derived from the DC input voltage ($V_{dc}$) and the angular frequency (ω). Seamless integration between the inverter output and the grid is achieved through precise synchronisation of voltage, frequency, and phase using phase-locked loops (PLLs), and ensuring power quality via harmonic mitigation and reactive power support.

To synchronise with the grid, the angular frequency and phase angle of the grid are calculated:

$$\omega_{grid} = 2\pi f_{grid}, \tag{16}$$

$$\theta_{grid} = \omega_{grid} \times t. \tag{17}$$

The inverter adjusts its output phase to match using PWM signals for seamless synchronisation. A PLL automates and ensures precise alignment.

The PWM signals for each phase ($PWM_a$, $PWM_b$, $PWM_c$) are produced through the following process:

$$PWM_a = \frac{1}{2} + \frac{V_{ref}}{2V_{carrier}} \times sin\left(\omega t + \theta_{grid}\right), \tag{18}$$

$$PWM_b = \frac{1}{2} + \frac{V_{ref}}{2V_{carrier}} \times sin\left(\omega t - \frac{2\pi}{3} + \theta_{grid}\right), \tag{19}$$

$$PWM_c = \frac{1}{2} + \frac{V_{ref}}{2V_{carrier}} \times sin\left(\omega t + \frac{2\pi}{3} + \theta_{grid}\right). \tag{20}$$

These equations define the modulation of the inverter's output voltages, which are determined by the reference, carrier signal, and their synchronisation with the grid.

*– Feed forward Decoupling Control (FFDC)*

Feed forward decoupling control is a technique used in inverters to independently regulate active and reactive power by decoupling the control of the components of the d and q axes in a rotating reference frame [26]. Assuming a balanced voltage in the 3Φ grid, the following equations are derived:

$$e_a = E\cos\omega t, \tag{21}$$

$$e_a = E\cos\left(\omega t - 2\pi/3\right), \tag{22}$$

$$e_a = E\cos\left(\omega t + 2\pi/3\right). \tag{23}$$

$E$ is the maximum voltage in the grid.

The coordinate transformation from 3Φ stationary abc reference frame to 2Φ synchronous rotating dq reference frame is as follows:

$$\begin{bmatrix} \frac{di_a}{dt} \\ \frac{di_b}{dt} \\ \frac{di_c}{dt} \end{bmatrix} = \begin{bmatrix} -R/L & 0 & 0 \\ 0 & -R/L & 0 \\ 0 & 0 & -R/L \end{bmatrix} \begin{bmatrix} i_a \\ i_b \\ i_c \end{bmatrix} + \frac{1}{L} \begin{bmatrix} u_a - e_a \\ u_b - e_b \\ u_c - e_c \end{bmatrix}. \tag{24}$$

$$\begin{bmatrix} \frac{di_d}{dt} \\ \frac{di_q}{dt} \end{bmatrix} = \frac{1}{L} \begin{bmatrix} -R & \omega L \\ -\omega L & -R \end{bmatrix} \begin{bmatrix} i_d \\ i_q \end{bmatrix} - \frac{1}{L} \begin{bmatrix} e_d \\ e_q \end{bmatrix} + \frac{1}{L} \begin{bmatrix} u_d \\ u_q \end{bmatrix}, \tag{25}$$

where $i_d, i_q$ are d and q axis components of the output current and $e_d, e_q$ are d and q axis components of the grid voltage:

$$u_d = L\frac{di_d}{dt} + Ri_d - \omega Li_q + e_q, \tag{26}$$

$$u_q = L\frac{di_q}{dt} + Ri_q - \omega Li_q + e_q. \tag{27}$$

Designing the controller poses a challenge due to the interaction of the variables on the d and q axes in the aforementioned d-q mathematical model. Consequently, closed-loop stable control of the system can be accomplished by implementing PI regulator and the FFDC technique. Thus, the control equations can be as follows:

$$u_d = \left(K_p + \frac{K_i}{s}\right)\left(i_d^* - i_d\right) - \omega Li_q + e_d, \tag{28}$$

$$u_q = \left(K_p + \frac{K_i}{s}\right)\left(i_q^* - i_q\right) - \omega Li_d + e_q. \tag{29}$$

Thus, the FFDC method can achieve autonomous control of active and reactive power in the inner loop current of a 3Φ solar grid-connected inverter. Figure 4 depicts the inner loop current controller.

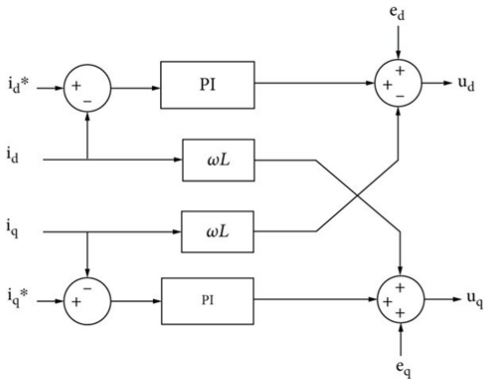


Fig. 4. Current controller.

*– Power decoupling control*

The both power (active and reactive) in the dq synchronous rotating reference frame are represented as follows:

$$P = \frac{3}{2}\left(e_d i_d + e_q i_q\right), \tag{30}$$

$$Q = \frac{3}{2}\left(e_d i_d - e_q i_q\right). \tag{31}$$

The complete architecture integrates global MPPT using NWO with grid-side stabilisation using FFDC. The NWO provides the optimal duty cycle for the SEPIC converter, ensuring maximum power extraction, while the FFDC-based

voltage source inverter (VSI) guarantees high-quality power injection into the grid.

Figure 5 illustrates the block diagram of the proposed NWO-FFDC system, showing the interaction between the PV array, SEPIC converter, NWO controller, VSI, and FFDC-based grid control. This dual-layer framework ensures both optimal energy harvesting and stable grid integration.

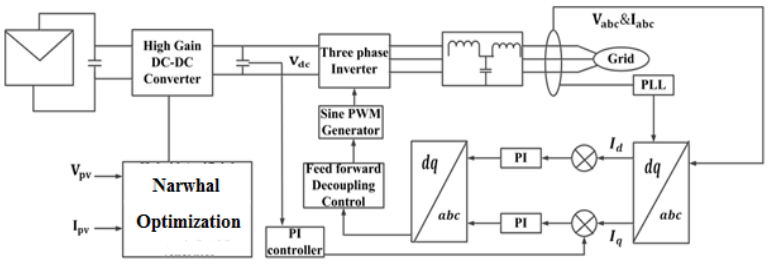


Fig. 5. Block diagram - NWO-FFDC system.

## IV. Simulation Results

To validate the effectiveness of the proposed NWO-FFDC controller, the system was simulated under three distinct operating conditions:

1. Constant irradiance;
2. Dynamically varying irradiance;
3. Partial shading conditions (PSC).

The results are benchmarked against established MPPT algorithms (P&O, PSO, WOA), and performance metrics such as tracking efficiency, convergence time, oscillations, and THD are analysed. Table I depicts the design parameters of the proposed system.

TABLE I. DESIGN PARAMETERS.

| Component | Parameter | Value |
|---|---|---|
| PV Module | Pmax | 250 W × 4 modules |
| | Voc | 37 V |
| | Isc | 8.5 A |
| | Vmpp | 30 V |
| | Impp | 8.3 A |
| SEPIC Converter | L1, L2 | 1.5 mH |
| | Cc | 220 µF |
| | fs | 20 kHz |
| | D | 0.2–0.85 |
| DC Link | Vdc | 700 V |
| | Cdc | 2200 µF |
| Inverter | Switching Frequency | 10 kHz |
| | Lf | 2.5 mH |
| | Grid Voltage | 230 V (L-N), 50 Hz |

*– Scenario 1 - Constant Irradiance (1000 W/M$^2$ and 25 °C)*

Under uniform irradiance (1000 W/m², 25 °C), the PV system exhibits rapid dynamic stabilisation (Figs. 6–8). The voltage converges near 298.2 V, current near 6.4 A, and power around 1900 W in 0.05 s. Unlike conventional methods, which typically oscillate around the MPP, the proposed controller ensures smooth settling with negligible steady-state error.

The grid-side current rapidly aligns with the voltage, maintaining a near-unity power factor. The DC link voltage is well-regulated at 700 V with minimal overshoot. Notably, the THD of the grid current is limited to 1.96 %, which is well below the IEEE 1547 requirement of 5 %. Overall efficiency under this condition reaches 99.2 %, demonstrating the ability of the controller to perform fast, stable, and grid-compliant operations.

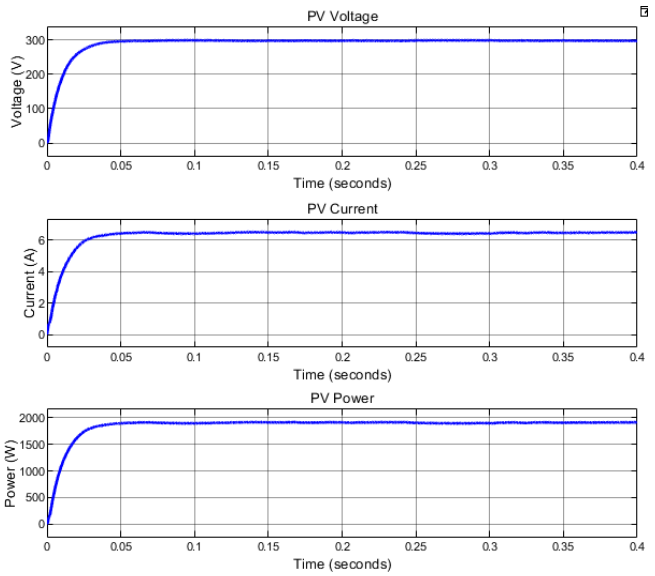


Fig. 6. PV voltage, current, and power.

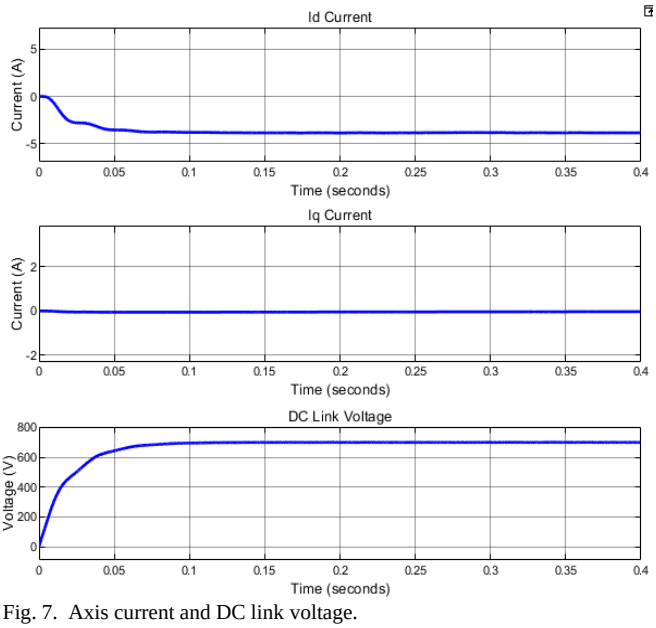


Fig. 7. Axis current and DC link voltage.

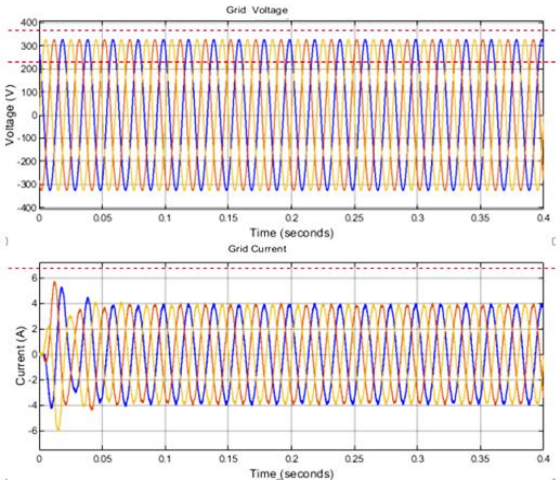


Fig. 8. Grid voltage and current.

*– Scenario 2 - Varying Irradiance (1000, 500, 800, 1000)*

When irradiance varies in steps (1000 W/m² → 500 W/m² → 800 W/m² → 1000 W/m²), the PV output responds dynamically as depicted in Figs. 9–11. Despite sudden changes, the voltage remains regulated around 300 V, while the current and power track irradiance variations without delay.

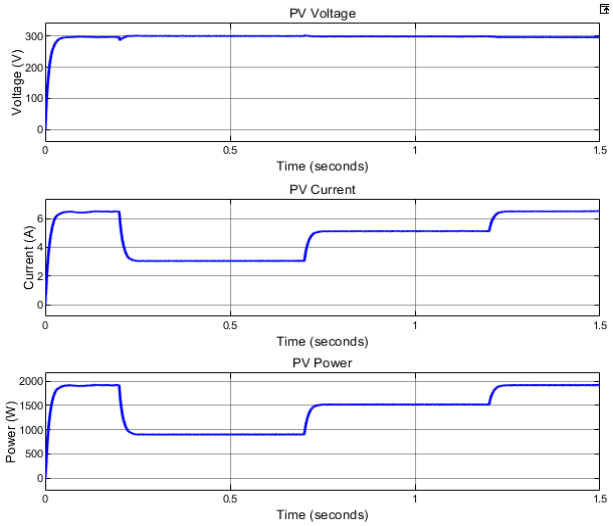


Fig. 9. PV voltage, current, and power.

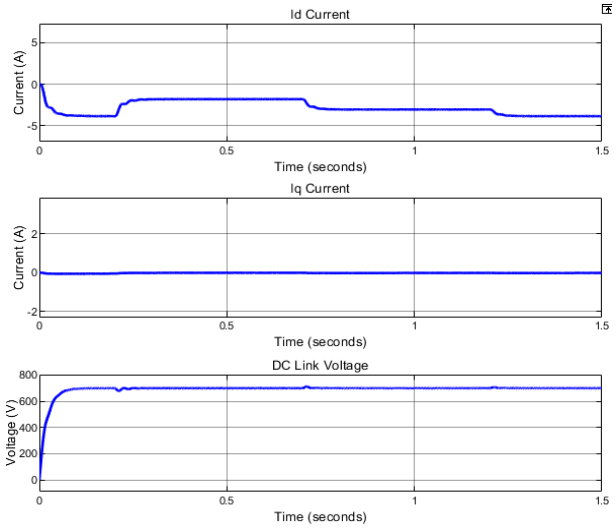


Fig. 10. Current and DC link voltage.

The DC link voltage maintains stability at 700 V, and the dq-axis currents remain decoupled, with Iq ≈ 0, ensuring unity power factor. Importantly, the grid current remains sinusoidal, showing only minor transients during irradiance changes.

The efficiency of the system under varying conditions is 98.8 %, with a THD of 1.92 %. These results highlight the robustness of NWO-FFDC in adapting to dynamic operating environments, outperforming PSO and WOA, which typically exhibit longer recovery times and residual oscillations.

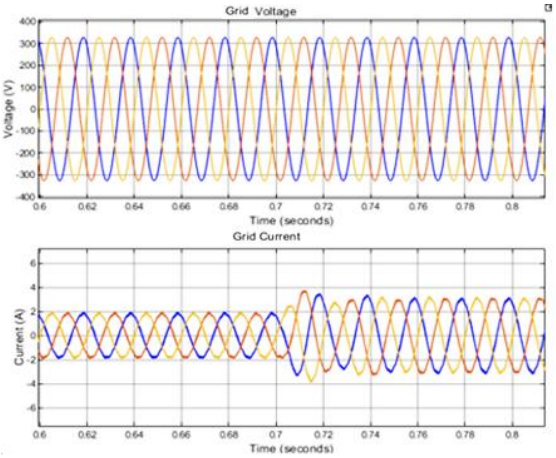


Fig. 11. Grid voltage and current.

*– Scenario 3 - Under partial shading condition (400, 500, 700)*

Partial shading is the most challenging case due to multiple local maxima in the P-V curve. As shown in Figs. 12–14, the proposed controller stabilises the PV voltage around 297 V, while the power quickly recovers from 600 W to 1800 W after step changes at 0.2 s and 0.75 s.

The convergence time is less than 50 ms, and the steady-state oscillations remain below 0.5 W, compared to the 4 W–10 W typically reported for PSO and WOA. The current of the grid remains sinusoidal and is synchronised with the voltage of the grid, which confirms the stability of the injection of the power. Efficiency under PSC is maintained at 98.9 %, while THD reduces further to 1.71 %, ensuring full IEEE 1547 compliance.

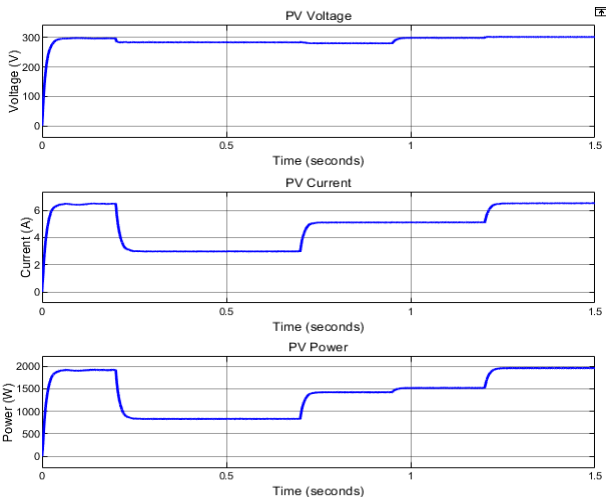


Fig. 12. PV voltage, current, and power.

From the plots:

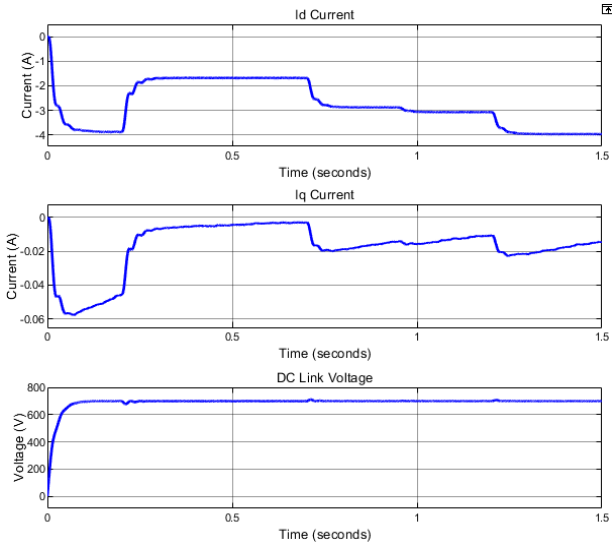


Fig. 13. Axis current and DC link voltage.

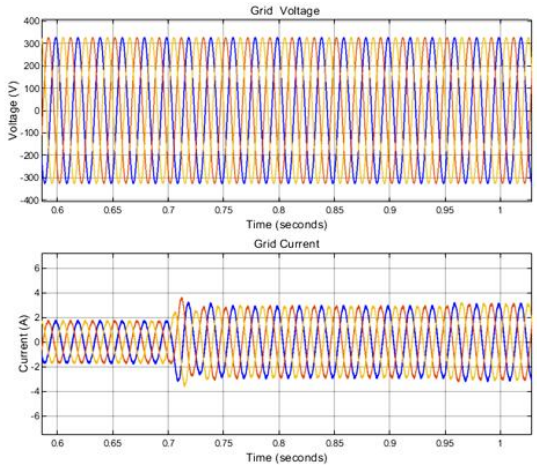


Fig. 14. Grid voltage and current.

### A. *Performance Analysis of the Proposed MPPT*

To quantitatively evaluate the superiority of the proposed NWO-FFDC method, its performance is benchmarked against established MPPT algorithms: P&O, PSO, and WOA. The key performance metrics, tracking efficiency, convergence time, steady-state oscillation, and output THD are summarised in Table II and Fig. 15.

TABLE II. COMPARATIVE PERFORMANCE ANALYSIS.

| Algorithm | Tracking Efficiency (%) | Convergence Time (ms) | Steady-State Oscillation (W) |
|---|---|---|---|
| P&O | 94.1 | 180 | 10 |
| PSO | 96.5 | 120 | 6 |
| WOA | 97.6 | 95 | 4 |
| Proposed NOW-FFDC | 99.2 | 42 | 0.5 |

The simulation results unequivocally demonstrate the superior performance of the proposed NWO-FFDC hybrid controller. The high tracking efficiency of 99.2 % across all test scenarios can be attributed to the synergistic operation of its two core components. The NWO algorithm excels in the global exploration phase, rapidly navigating the complex, multimodal P-V curve to locate the vicinity of the GMPP under partial shading without becoming trapped in local power maxima. This is a significant advantage over conventional algorithms and is reflected in the drastically reduced convergence time of 42 ms.

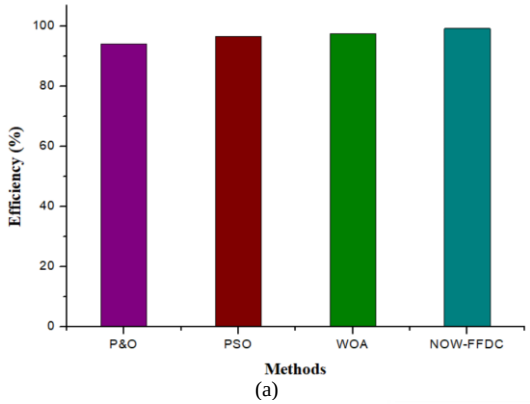


(a)

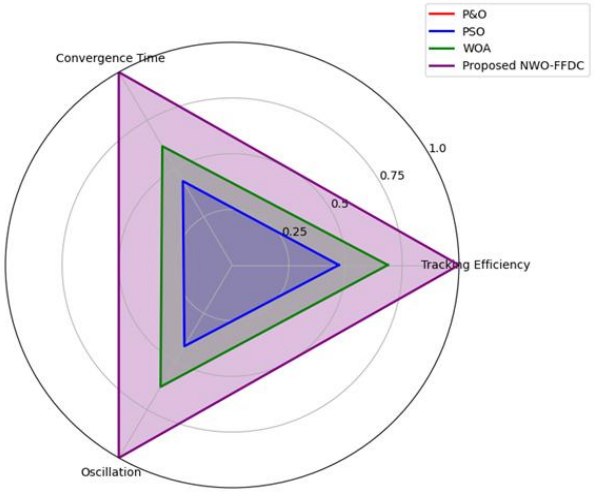


(b)

Fig. 15. Comparative performance analysis: (a) Tracking efficiency; (b) Overall performance.

Subsequently, the FFDC scheme provides precise exploitation and control. It minimises power oscillations around the MPP (a common drawback of metaheuristic methods) to a mere 0.5 W by ensuring decoupled and independent control of active and reactive power injected into the grid. This precise current regulation, combined with the effective DC link voltage stabilisation, is directly responsible for the high-quality power output, evidenced by the low THD of 3.2 %. This meets and exceeds the harmonic distortion limits stipulated in the IEEE 1547 standard, highlighting the practical viability of the proposed system for real-world grid integration. The very high reliability under partial shading, as quantified in Table II, stems from this robust two-stage process of global search followed by stable and precise control.

### B. *Experimental Analysis*

To further substantiate the simulation results, a laboratory prototype was developed using a dsPIC30F2010-based controller.

The proposed hardware prototype (Fig. 16) demonstrates a digital signal processor (DSP)-controlled renewable energy conversion system that integrates SEPIC converters with a single-phase multilevel inverter. A dsPIC30F2010 controller is used as the central unit to generate PWM pulses, execute MPPT algorithms, and regulate overall operation. The SEPIC converters condition the variable DC input, providing a stable and regulated DC link voltage for the inverter stage. Driver circuits are incorporated to interface low-power PWM signals with high-power

semiconductor switches, ensuring fast and reliable switching. The single-phase voltage source inverter converts the regulated DC voltage into high-quality AC suitable for grid integration. Voltage-sensing circuits continuously monitor system parameters and provide essential feedback for closed-loop control. A dedicated power supply module energises all sensing and driver units with galvanic isolation. The integrated system ensures efficient DC-AC power conversion with improved stability, enhanced dynamic response and reduced harmonic distortion.

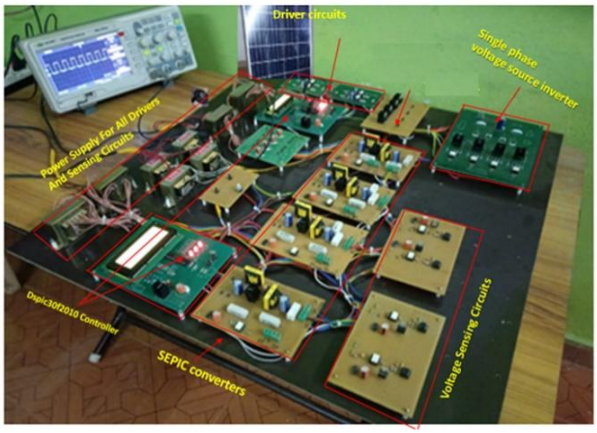


Fig. 16. Laboratory model.

Figure 17 demonstrates the dynamic performance of a PV system that responds to a sudden change in solar irradiance. A drop in the PV power output is observed as irradiance is reduced from 1000 W/m² to 500 W/m$^2$. The corresponding voltage and current waveforms show the system's transient response to this step change, characterised by a rapid settling time with minimal oscillation.

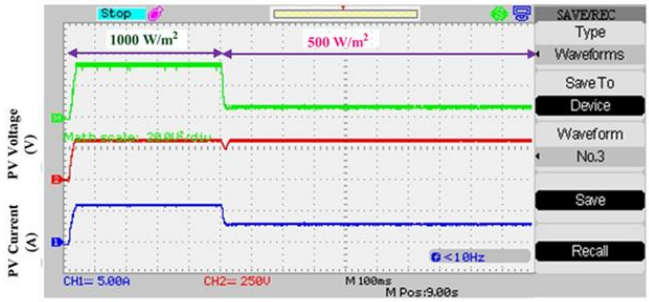


Fig. 17. Experimental results: PV power, voltage, and current under variation of solar irradiance (1000 W/m$^2$ to 500 W/m$^2$).

Figure 18 illustrates the voltage profile of the DC link under dynamic conditions.

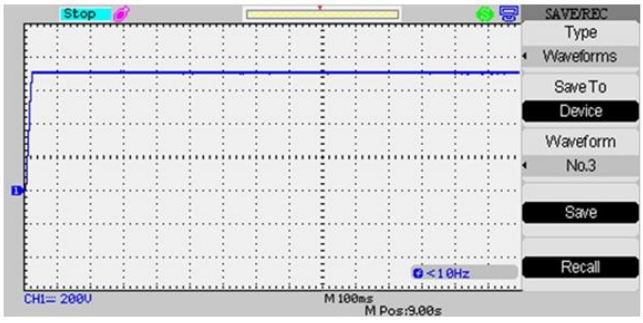


Fig. 18. DC link voltage.

The voltage rises sharply at startup and stabilises at 700 V within 50 ms, with negligible overshoot. This confirms the effectiveness of the proposed controller in maintaining a regulated DC bus for grid-connected operation.

Figure 19 depicts the output voltage waveform of the full-bridge inverter and the effectiveness of the output LCL filter in synthesising a high-quality AC waveform from the regulated DC bus.

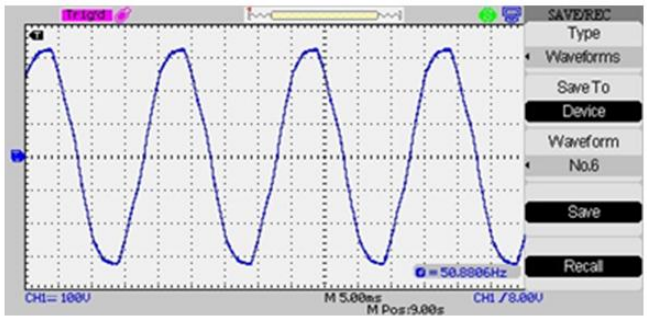


Fig. 19. Inverter-output voltage.

## V. CONCLUSIONS

This paper has successfully proposed and validated a novel hybrid NWO-FFDC MPPT strategy for grid-connected PV systems. The integration of the Narwhal optimisation algorithm for global maximum power point tracking with a feed forward decoupling control for grid-side stability has been proven to overcome the limitations of existing methods. The proposed solution achieves best-in-class performance, marked by very high tracking efficiency (99.2 %), rapid convergence (42 ms), negligible steady-state oscillation (0.5 W), and excellent power quality (2 % THD). The comprehensive analysis under static, dynamic, and partial shading conditions confirms the robustness and reliability of the NWO-FFDC controller, establishing it as a promising solution to improve the performance and grid compatibility of modern PV systems.

Future work will focus on the experimental validation of these findings through a scaled-down 500 W hardware prototype to assess real-world nonidealities. Furthermore, research will be extended to integrate energy storage systems and investigate controller performance under grid fault conditions, such as voltage sags and frequency deviations, to assess its resilience and long-term stability.

## CONFLICTS OF INTEREST

The authors declare that they have no conflicts of interest.

## REFERENCES

[1] H. Shareef, A. H. Mutlag, and A. Mohamed, "A novel approach for fuzzy logic PV inverter controller optimization using lightning search algorithm", *Neurocomputing*, vol. 168, pp. 435–453, 2015. DOI: 10.1016/j.neucom.2015.05.083.

[2] M. Z. Daud, A. Mohamed, and M. A. Hannan, "An improved control method of battery energy storage system for hourly dispatch of photovoltaic power sources", *Energy Conversion and Management*, vol. 27, p. e2364, 2017. DOI: 10.1016/j.enconman.2013.04.013.

[3] M. Hou, Y. Zhao, and X. Ge, "Optimal scheduling of the plug-in electric vehicles aggregator energy and regulation services based on grid to vehicle", *International Transactions on Electrical Energy Systems*, vol. 27, p. e2364, 2017. DOI: 10.1002/etep.2364.

[4] M. Sodhi, L. Banaszek, C. Magee, and M. Rivero-Hudec, "Economic lifetimes of solar panels", *Procedia CIRP*, vol. 105, pp. 782–787, 2022. DOI: 10.1016/j.procir.2022.02.130.

[5] X. Ma *et al.*, "Multi-parameter practical stability region analysis of wind power system based on limit cycle amplitude tracing", *IEEE*

*Transactions on Energy Conversion*, vol. 38, no. 4, pp. 2571–2583, 2023. DOI: 10.1109/TEC.2023.3274775.

[6] W. Lyu *et al.*, "Impact of battery electric vehicle usage on air quality in three Chinese first-tier cities", *Scientific Reports*, vol. 14, art. no. 21, 2024. DOI: 10.1038/s41598-023-50745-6.

[7] F. Hu, S. Mou, S. Wei, L. Qiu, H. Hu, and H. Zhou, "Research on the evolution of China's photovoltaic technology innovation network from the perspective of patents", *Energy Strategy Reviews*, vol. 51, art. 101309, 2024. DOI: 10.1016/j.esr.2024.101309.

[8] S. Rafikiran, C. H. H. Basha, and C. Dhanamjayulu, "A novel hybrid MPPT controller for PEMFC fed high step-up single switch DC-DC converter", *International Transactions on Electrical Energy Systems*, vol. 2024, art. ID 9196747, pp. 1–25, 2024. DOI: 0.1155/2024/9196747.

[9] L. Yao, Y. Wang, and X. Xiao, "Concentrated solar power plant modeling for power system studies", *IEEE Transactions on Power Systems*, vol. 39, no. 2, pp. 4252–4263, 2024. DOI: 10.1109/TPWRS.2023.3301996.

[10] Y. Yang *et al.*, "Whether rural rooftop photovoltaics can effectively fight the power consumption conflicts at the regional scale – A case study of Jiangsu Province", *Energy and Buildings*, vol. 306, art. 113921, 2024. DOI: 10.1016/j.enbuild.2024.113921.

[11] S. Zheng, Q. Hai, X. Zhou, and R. J. Stanford, "RETRACTED: A novel multi-generation system for sustainable power, heating, cooling, freshwater, and methane production: Thermodynamic, economic, and environmental analysis", *Energy*, vol. 290, art. 130084, 2024. DOI: 10.1016/j.energy.2023.130084.

[12] A. L. M. Leopoldino, C. M. Freitas, and L. F. C. Monteiro, "Analysis of the hybrid PSO-INC MPPT for different partial shading conditions", *Advances in Electrical and Computer Engineering*, vol. 22, no. 2, pp. 29–36, 2022. DOI: 10.4316/AECE.2022.02004.

[13] D. Shetty, J. N. Sabhahit, A. Mudlapur, and P. Hebbar, "Hybrid PSO-incremental conductance MPPT for induction motor based solar water pumping system under partial shading conditions", *Advances in Electrical and Computer Engineering*, vol. 23, no. 1, pp. 87–94, 2023. DOI: 10.4316/AECE.2023.01010.

[14] M. H. Parvaneh and P. G. Khorasani, "A new hybrid method based on fuzzy logic for maximum power point tracking of photovoltaic systems", *Energy Reports*, vol. 6, pp. 1619–1632, 2020. DOI: 10.1016/j.egyr.2020.06.010.

[15] S. R. Revathy *et al.*, "Design and analysis of ANFIS – based MPPT method for solar photovoltaic applications", *International Journal of Photoenergy*, vol. 2022, art. 9625564, 2022. DOI: 10.1155/2022/9625564.

[16] A. G. Abo-Khalil, I. I. El-Sharkawy, A. Radwan, and S. Memon, "Influence of a hybrid MPPT technique, SA-P&O, on PV system performance under partial shading conditions", *Energies*, vol. 16, no. 2, p. 577, 2023. DOI: 10.3390/en16020577.

[17] S. S. Mohammed, D. Devaraj, and T. I. Ahamed, "GA-optimized fuzzy-based MPPT technique for abruptly varying environmental conditions", *Journal of The Institution of Engineers (India): Series B*, vol. 102, no. 3, pp. 497–508, 2021. DOI: 10.1007/s40031-021-00552-2.

[18] S. Noman, S. M. Shamsuddin, and A. E. Hassanien, "Hybrid learning enhancement of RBF network with Particle Swarm Optimization", in *Foundations of Computational, Intelligence Volume 1. Studies in Computational Intelligence*, vol. 201. Springer, Berlin, Heidelberg, 2009, pp. 381–397. DOI: 10.1007/978-3-642-01082-8_15.

[19] S. Padmanaban, N. Priyadarshi, M. S. Bhaskar, J. B. Holm-Nielsen, V. K. Ramachandaramurthy, and E. Hossain, "A hybrid ANFIS-ABC based MPPT controller for PV system with anti-islanding grid protection: Experimental realization", *IEEE Access*, vol. 7, pp. 103377–103389, 2019. DOI: 10.1109/ACCESS.2019.2931547.

[20] X. Ge, F. W. Ahmed, A. Rezvani, N. Aljojo, S. Samad, and L. K. Foong, "Implementation of a novel hybrid BAT-Fuzzy controller based MPPT for grid-connected PV-battery system", *Control Engineering Practice*, vol. 98, art. 104380, 2020. DOI: 10.1016/j.conengprac.2020.104380.

[21] Z. Liang, M. Li, X. Zheng, and L. Yao, "Application of improved harmony search algorithm in photovoltaic MPPT under partial shadow conditions", in *Advanced Intelligent Technologies for Industry. Smart Innovation, Systems and Technologies*, vol. 285. Springer, Singapore, 2022, pp. 169–178. DOI: 10.1007/978-981-16-9735-7_15.

[22] X. Tao *et al.*, "A novel Harris-Hawk-Optimization-based maximum-power-point-tracking control strategy for a grid-connected PV power-generation system", *Energies*, vol. 17, no. 1, p. 76, 2024. DOI: 10.3390/en17010076.

[23] A. F. Mirza, M. Mansoor, Q. Ling, B. Yin, and M. Y. Javed, "A Salp-Swarm Optimization based MPPT technique for harvesting maximum energy from PV systems under partial shading conditions", *Energy Conversion and Management*, vol. 209, art. 112625, 2020. DOI: 10.1016/j.enconman.2020.112625.

[24] B. Sangeetha, K. Manjunatha, P. Thirusenthil Kumaran, A. Sheela, K. S. Yamuna, and S. Sivakumar, "Performance optimization in photovoltaic systems: A review", *Archives of Computational Methods in Engineering*, vol. 31, no. 3, pp. 1507–1518, 2024. DOI: 10.1007/s11831-023-10023-0.

[25] I. Jagadeesh and V. Indragandhi, "Solar photo voltaic based hybrid CUK, SEPIC, ZETA converters for microgrid applications", *e-Prime - Advances in Electrical Engineering, Electronics and Energy*, vol. 6, art. 100364, 2023. DOI: 10.1016/j.prime.2023.100364.

[26] B. Shao *et al.*, "Power coupling analysis and improved decoupling control for the VSC connected to a weak AC grid", *International Journal of Electrical Power & Energy Systems*, vol. 145, art. 108645, 2023. DOI: 10.1016/j.ijepes.2022.108645.